

Thermal wave interferometry for measuring the thermal diffusivity of thin slabs

F. CERNUSCHI, A. FIGARI

ENEL S.p.A. SRI, Via Reggio Emilia, 39, 20090 Segrate Italy
E-mail: Cernuschi@cram.enel.it

L. FABBRI

European Commission, Joint Research Centre, P.O. Box 2, 1755 ZG Petten, The Netherlands

Thermal wave interferometry applied to the evaluation of thermal diffusivity of freestanding coatings and single layers is herewith presented. Measurements on a set of eight different materials (oxides free copper, an aluminium alloy, Armco iron, AISI 316 stainless steel, Nimonic90 and IN738 nickel based alloys and Ytria partially stabilised Zirconia coatings) have been carried out. The corresponding thermal diffusivity values cover a very large range (about three order of magnitude). A comparison of 1D and 3D models has been done in order to optimise the main measurement parameters. Sample thickness, heating beam size and modulation frequency range have been selected in order to maximise the photothermal signal and its phase variation as a function of the frequency. Experimental results give evidence of a very good agreement between literature and experimental values for all samples confirming the capability of this technique for measuring the thermal diffusivity of thin slabs. © 2000 Kluwer Academic Publishers

1. Introduction

The thermal diffusivity α plays a key role in many applications when heat transfer phenomena are involved. Since the last century, many different methods for measuring this property have been developed [1, 2].

At the present days, the laser flash method [3–6] is considered the standard technique for thermal diffusivity measurements of solids materials.

This method consists in heating a sample by a short laser pulse and detecting the temperature evolution on its rear surface. One limitation of the laser-flash method is related to the need of accurate and specific sample geometrical requirements, typically a thin small cylinder.

In the last few decades, several photothermal techniques [7] have been developed for measuring thermal diffusivity. In particular, the mirage method has been widely applied mainly for measuring the thermal diffusivity in thermally thick materials [8–11]. This technique is based on the periodical heating (with a frequency f) of a sample by a modulated laser beam (pump beam) which generates a thermal wave within the sample.

Modulated thermal gradient and consequent gradient in the refractive index of air are induced in the air close to the sample: the periodical deflection of a probe beam grazing along the sample surface is measured by a position sensor.

A precise scanning of the thermal wave field by varying the distance x_0 between pump and probe laser beams gives the thermal wavelength and the thermal diffusivity.

In particular, in the zero crossing technique [9, 10], x_0 is the separation between the points corresponding to a signal phase shift of $\pm\pi/2$ with respect to the spot centre $x = 0$. In the arbitrary phase shift technique [12, 13], $x_0(\phi^*)$ is the separation between the points corresponding to an arbitrary phase shift ϕ^* of the signal relative to the spot centre.

In both techniques α is linked to the slope of the experimental curve of x_0 versus $f^{-1/2}$.

An original approach to photothermal techniques is based on wave optics [14, 15].

Starting from the pioneering works of Bennett and Patty and Almond [16, 17], thermal wave interferometry (TWI) in 1D-approximation [7] has been widely applied for coating thickness or thermal diffusivity evaluation [17–19]. Similarly to the previous technique, TWI is based on the periodical heating of a sample (typically by a modulated laser beam). The two-layer structure of the coated sample produces a change of the ac-component of the temperature with respect to an uncoated surface: this change of the surface temperature can be detected by an IR detector.

In the last few years, TWI in 3D-approximation has been considered in order to measure also the in-plane thermal diffusivity of bulk materials [20, 21].

Photothermal reflectance technique [22–26] has been successfully applied to measure thermal diffusivity of thin films as well as bulk materials.

Also transient photothermal techniques have successfully applied for measuring thermal diffusivity of both bulk [27], coatings [19, 28] and free standing layers [29]. In this cases, sample surface is heated by an

optical pulse (Dirac or single square wave shaped) and the time evolution of the surface temperature is monitored by an IR detector.

All these methods (but not laser flash method) are single sided and contactless. Mirage and reflectance methods require a high flatness of sample surface but not TWI.

This pushes to extend the application of TWI also to thermal diffusivity evaluation of thin slabs.

In this work, TWI technique is applied to evaluate thermal diffusivity of single layers and free standing coatings of some different materials with thermal diffusivities ranging in a quite large range: between c.a. 0.001 and 1.1 cm²/s. In order to optimise sample thickness, as well as measurement parameters (i.e. frequency range and laser beam size) a specific study on the validity limits of the 1D approximation has been performed.

2. Photothermal technique: Theoretical remarks

Thermal Wave Interferometry is a well-established technique for the measure of the thickness and the thermal diffusivity of coatings and is specifically well suited for thermal barrier coatings [7, 16, 17, 19]. When a thermal wave is generated within solid multilayered samples by intensity modulated optical excitation (typically a continuous wave laser), the propagation of this wave is affected by the presence of the thermal mismatch at the coating-substrate interface. In particular, as thermal waves behave like common waves, they are partially reflected and transmitted at the separation surface of the two different materials. The analysis of the temperature distribution on the sample surface gives information on both the coating thickness and its thermal diffusivity.

For a two layer sample heated uniformly by a temporally modulated optical source at an angular frequency $\omega (=2\pi f)$, the ac-component of the surface temperature depends on both the coating thickness L and the thermal diffusivity, $\alpha = \frac{k}{\rho C}$, as follows [16, 17]:

$$T(0, t) = \frac{I_0}{k_1 \sigma_1} \frac{(1 + \text{Re}^{-2\sigma_1 L})}{(1 - \text{Re}^{-2\sigma_1 L})} e^{j\omega t} \quad (1)$$

where $\sigma_1 = (1 + j)\sqrt{\frac{\omega}{2\alpha_1}}$ (j the imaginary unit), and ρ , C , k and I_0 are the density, the thermal capacity, the thermal conductivity and the power density respectively; $R = \frac{\varepsilon_1 - \varepsilon_2}{\varepsilon_1 + \varepsilon_2}$ (where $\varepsilon_i = \sqrt{\rho_i C_i k_i}$ is the thermal effusivity) is the thermal wave reflection coefficient at the interface where subscripts 1 and 2 refer to coating and substrate, respectively. $\sqrt{\frac{\omega}{2\alpha_1}}$ is the thermal diffusion length μ and represents, in Equation 1, the decay constant of the thermal wave damping (i.e. the depth where the initial magnitude of the thermal wave reduces by a $1/e$ factor). Furthermore, from Equation 1 it is possible to define both amplitude A and phase $\Delta\phi$ as follows [16]:

$$A = \left(\frac{e^{4h} + 2\text{Re}^{2h} \cos(2h) + R^2}{e^{4h} - 2\text{Re}^{2h} \cos(2h) + R^2} \right)^{1/2}$$

$$\Delta\phi = \arctan\left(\frac{e^{-2h}(e^{4h} - R^2)}{2R \sin(2h)} \right) \quad (2)$$

where $h = L/\mu$ is the normalised thickness of the first layer.

Experimentally, a non linear regression technique allows to evaluate, from one of the two expressions of Equation 2, L^2/α and R . If L is known, thermal diffusivity α can be obtained. In order to perform a multiparametric non linear best fitting, data referring to measurements carried out at different frequencies are required. Phase measurements are usually preferred to the amplitude ones because f is less sensitive to optical features of the sample surface as well as to laser power variation during the measurement.

As an example, Fig. 1 shows both theoretical curves for amplitude and phase as a function of the normalised coating thickness (h) for R values ranging between -1 and 1 .

When the beam radius \mathfrak{R} (defined as the distance where intensity reduces to $1/e$ of value at the beam centre) can not be supposed infinite in respect of the area a imaged by the IR detector, the one-dimensional solution of the Fourier equation is no more applicable. The three dimensional ac temperature of sample surface for an harmonic gaussian beam \mathfrak{R} is [30]:

$$\bar{T}_{3D}(r) = \frac{I_0 \mathfrak{R}^2}{2\pi k_1} \int_0^\infty \frac{J_1(\lambda a) \exp\left(-\frac{\lambda^2 \mathfrak{R}^2}{4}\right)}{\lambda a \sigma_1(\lambda)} \times \left[\frac{1 - \Gamma_{3D}(\lambda) \exp(-2\sigma_1(\lambda)L)}{1 + \Gamma_{3D}(\lambda) \exp(-2\sigma_1(\lambda)L)} \right] J_0(\lambda r) \lambda d\lambda \quad (3)$$

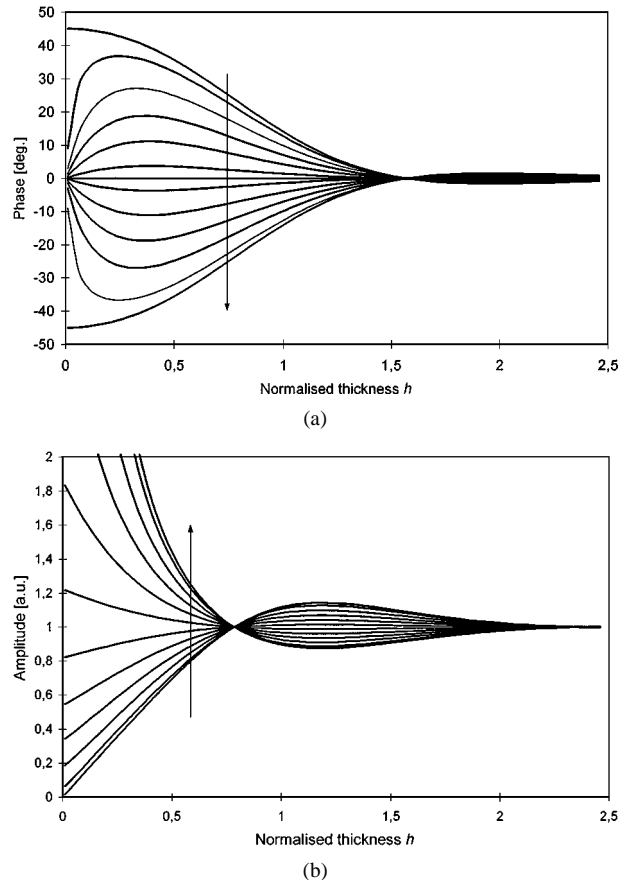


Figure 1 Phase (a) and amplitude (b) of the ac component of temperature versus the normalised thickness h for different values of the reflection coefficient R ranging from -1 to 1 (in the sense of the arrow).

where J_0 and J_1 are zero and first order Bessel functions of first kind respectively,

$$\sigma_i(\lambda) = \left[\lambda^2 + \frac{j\omega}{\alpha_i} \right]^{1/2} \quad i = 1, 2 \quad (4)$$

are the complex wave numbers and

$$\Gamma_{3D}(\lambda) = \frac{1 - b_{3D}(\lambda)}{1 + b_{3D}(\lambda)} \quad \text{where} \quad b_{3D}(\lambda) = \frac{k_2 \sigma_2(\lambda)}{k_1 \sigma_1(\lambda)} \quad (5)$$

is the thermal wave reflection coefficient.

Main differences of Equations 3–5 if compared with the one-dimensional case are related to the frequency dependence on λ of complex wave numbers and consequently also of the reflection coefficient Γ_{3D} . As it is more practical to use the one-dimensional approximation, an accurate analysis to establish the validity limits of this approximation should be performed. This could be done comparing Equations 1 and 3 as a function of frequency range, beam size and layer thickness.

3. Experimental

3.1. Materials

The samples selected in the present work have been chosen in order to cover a very large range of thermal diffusivity values (ca. three orders of magnitude). In particular the following materials have been considered:

Two free standing Ytria Partially Stabilized Zirconia (YPSZ) coatings. The first, hereafter called APS, was Air Plasma Sprayed (APS) while the second, EBPVD, was deposited by Electron Beam Vapour Physical Deposition EB-PVD. APS coating has been deposited on an AISI304 stainless steel by Flame Spray using Starck Amperit 825.0 (H. C. Starck, Germany) ($ZrO_2 + 7 \text{ wt\% } Y_2O_3$) powder and a Metco 3M gun. EBPVD coating has been deposited on an AISI304 stainless steel by Chromalloy U.K. following their standard procedure. Both coatings have been detached from the substrate by a chemical attack.

Six metallic layers made of oxides free electrolytic copper, the aluminium alloy UNI3571, Armco Iron, AISI316 stainless steel, NIMONIC90 and IN738 nickel base alloys have been selected. In particular, Table I reports the composition of these alloys.

Sample thickness and thermal diffusivity values as reported in data sheets or in literature are collected in Table II.

As zirconia is translucent to the optical radiation (and since TWI model requires total absorption on the sam-

TABLE II Thickness and literature values of thermal diffusivity of samples

	Thickness [μm]	Thermal diffusivity [$10^{-4} \text{ m}^2/\text{s}$]
Electrolytic Copper	1025 ± 4	1.16 [7]
Aluminium alloy UNI3571	1058 ± 1	0.64 [31]
ARMCO Iron	820 ± 4	0.16–0.25 [32,33]
AISI316 stainless steel	610 ± 5	0.0348 [7]
NIMONIC90 Nickel base alloy	507 ± 4	0.031 [34]
IN738 Nickel base alloy	415 ± 4	0.026–0.04 [33, 35]
EBPVD YPSZ	625 ± 10	0.0086 [36]
APS YPSZ	282 ± 19	0.0020–0.0045 [19, 32, 33, 35, 37]

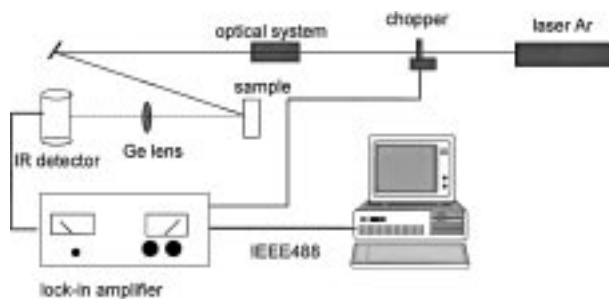


Figure 2 TWI experimental set-up.

ple surface (within a depth that is negligible if compared to the thermal diffusion length), a thin layer of gold ($<50 \text{ nm}$ thick) has been deposited on the sample surface by sputtering.

To avoid the reflection of laser visible light, metallic samples have been lightly sand blasted and then a thin graphite layer ($<50 \text{ nm}$ thick) has been evaporated on their surface.

3.2. TWI experimental set-up

Fig. 2 shows the TWI experimental set-up: the heating source is a 5W Ar ion laser (Spectra Physics 2020). The intensity, always lower than 1.5 W, was modulated using a high stability mechanical chopper (HMS Elek-troniK mod. 220-RG). An optical system allowed to expand the laser beam on the sample surface so that the one-dimensional approximation was guaranteed [30]. The infrared radiation emitted by the sample surface was collected and focused on a $Hg_{1-x}Cd_xTe$ infrared detector (EG&G Judson) by using a Germanium lens. The detector active area was $0.1 \text{ mm} \times 0.1 \text{ mm}$. The

TABLE I Chemical composition (wt.%) of metallic samples

	Al	Cu	Si	Mg	Mn	Fe	Cr	Co	Ni	Ti	Mo	W	Ta	C	P	S	Sn	Zn
Copper		>99.8																
UNI3571	bal.		0.8–1.0	0.5–0.85	0.25–0.7	0.45	<0.1			<0.1								<0.1
ARMCO Iron		0.01		0.01	0.01	99.94	0.01		0.005		0.001							0.001
AISI316			<1		<2	bal.	16–18			10–14				<0.1	<0.045	<0.03		
NIMONIC 90	1–2	0.2	1		1	1.5	18–21	15–21	bal.	2–3				<0.13				<0.015
IN738		3.4					16	8.5	bal.	3.4	1.75	2.5	1.75	0.17				

signal was amplified firstly by a dc-coupled low noise transimpedance preamplifier and then by a lock-in amplifier (EG&G mod. 5501). A time averaging procedure with statistic treatment of the data and subsequent coating thermal diffusivity evaluation was performed under the control of a proprietary PC program.

3.3. Optimisation of measurement parameters

As already stated, the modulation frequency range as well as the laser beam size have been modified as a function of the sample tested, in order to guarantee the validity of the one-dimensional heating approximation [see Equation 1].

As a matter of fact, for optimising the experimental parameters it should be taken into account that the sample thickness is obtained as the best compromise between signal amplitude and phase variation in the frequency scanning measurement. In fact, as shown in Fig. 1a amplitude strongly decreases as the L/μ is increased; on the contrary, maximum phase variation (see Fig. 1b) takes place for L/μ in the range 0.3–1.5.

Furthermore, as the thermal diffusion length μ depends on both the thermal diffusivity of the material and the modulation frequency f , the sample thickness L should be chosen to satisfy the already mentioned condition on L/μ . But the photothermal signal always decreases as the modulation frequency f increases. This means that f should be always chosen as low as possible. Since the lower f the longer μ , in order to guarantee the one-dimensional heating approximation the laser beam size should be expanded in suitable way. But expanding the beam, the power density reduces as the square of the beam radius and consequently the photothermal signal as well.

In order to optimise the experimental parameters, some preliminary simulations have been performed comparing phase as a function of modulation frequency f in one and three dimensional approximations. In this way we have selected the minimum beam size for scanning the frequency within the range either satisfying the one-dimensional approximation or corresponding to a L/μ range of 0.3–1.5.

As example of these theoretical simulations, for some of the studied samples Figs 3 and 4 show phase versus frequency curves in three dimensional and one dimensional approximations for different beam sizes.

Beam dimension was experimentally measured using a method described in details elsewhere [30].

Table III summarises frequency ranges and beam radius used for carrying out measurements on samples.

From the experimental point of view, beam sizes and modulation frequencies have been chosen to limit the phase difference between one and three dimensional models to 1 degree. In particular for all samples but copper and aluminium the phase difference results always smaller than 0.9 degrees and 0.07 degrees at the lowest and at the highest modulation frequency respectively. For the two most diffusive materials phase difference ranges from 1.5 to 0.3 degrees. These values correspond to the experimental uncertainty.

TABLE III Main experimental TWI parameters chosen for the samples

Sample	Modulation Frequency range [Hz]	Radius beam size [μm]
YPSZ-APS	1–30	5043
YPSZ-EBPVD	1–10	5043
Electrolytic Copper	30–85	7532
UNI3571 Aluminium alloy	20–70	7532
Armco Iron	10–30	7532
AISI316 stainless steel	1–20	5043
NIMONIC90 nickel alloy	3–20	5043
IN738 nickel alloy	3–20	5043

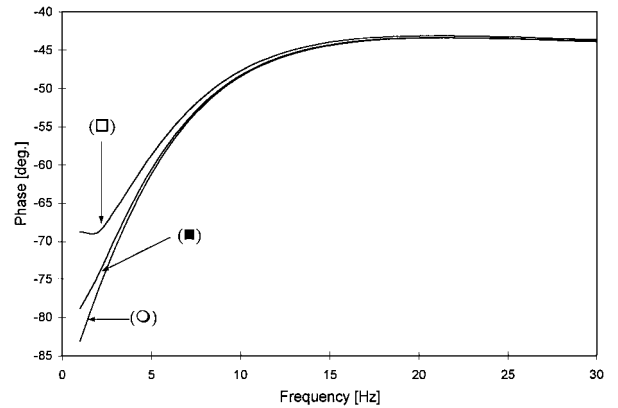


Figure 3 Theoretical phase versus modulation frequency curves as a function of the heating beam size. Curves refer to one-dimensional case (O), to three dimensional case with a $R = 5000 \mu\text{m}$ (■), and $R = 2500 \mu\text{m}$ (□) for IN738 sample. Three dimensional curves have been computed using Equation 3 where $a = 100 \mu\text{m}$.

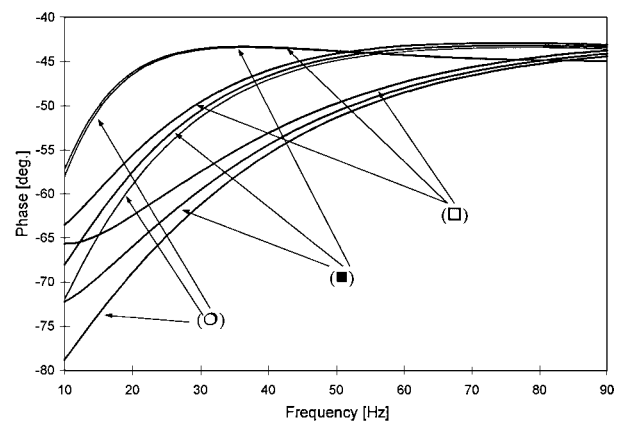


Figure 4 Theoretical phase versus modulation frequency curves as a function of the heating beam size. Curves refer to one-dimensional case (O), to three dimensional case with a $R = 5000 \mu\text{m}$ (■), and $R = 7500 \mu\text{m}$ (□) for Armco iron (upper curves), UNI3571 (intermediate curves) and electrolytic copper (lower curves) samples. Three dimensional curves have been computed using Equation 3 where $a = 100 \mu\text{m}$.

3.4. Experimental uncertainty

In order to reduce the statistical uncertainty of the measurement, at each frequency, phase measurements were carried out for a period of time T_m corresponding to the sum of a fixed time T_{fix} (usually 40 seconds) and a variable time expressed as a function of the number of periods; thus T_m resulted:

$$T_m = T_{\text{fix}} + \text{Periods}/f \quad (6)$$

TABLE IV Thermal diffusivity values as measured by TWI on samples and as reported in literature

	Thermal diffusivity Experimental [10^{-4} m ² /s]	Experimental uncertainty [%]	Thermal diffusivity Literature values [10^{-4} m ² /s]
Electrolytic Copper	1.15 ± 0.08	7	1.16 [2]
Aluminium alloy UNI3571	0.63 ± 0.02	3	0.56–0.8 [31]
ARMCO Iron	0.18 ± 0.01	5	0.16–0.25 [32, 33]
AISI316 Stainless steel	0.037 ± 0.001	3	0.0348 [7]
NIMONIC90 Nickel base alloy	0.033 ± 0.001	3	0.031 [34]
IN738 Nickel base alloy	0.028 ± 0.001	4	0.026–0.04 [33, 35]
EBPVD YPSZ	0.0081 ± 0.0001	1	0.0086 [36]
APS YPSZ	0.0028 ± 0.0001	4	0.0020–0.0050 [19, 32, 33, 35, 37]

Generally periods ranged from 10 to 60 as a function of the considered material.

At each modulation frequency data were acquired at time intervals longer than three times the lock-in amplifier time constant τ set up for the measurement; in this way single measurements could be considered statistically not correlated one to each other.

For the standard deviation:

$$\sigma = \sqrt{\frac{\sum_{i=1}^N (x_i - \bar{x})^2}{N(N-1)}} \quad (7)$$

N ranged from 20 to 70 as a function of the modulation frequency, of the lock-in time constant τ and of the number of periods set up in the acquisition software.

After completing the frequency scanning, as the uncertainty of the experimental data varied with the frequency, multiparametric weighted non linear fitting of phase versus frequency should be applied in order to estimate the thermal diffusivity. This was done applying a Levenberg-Marquardt procedure for minimising the expression:

$$\chi^2(\alpha, L, R, K) = \sum_{i=1}^N \frac{[\phi(\alpha, L, R, K) - \phi_i]^2}{\sigma_i^2} \quad (8)$$

where K is an arbitrary additive constant added to the phase, $\phi(\alpha, L, R, K)$ is the analytical solution of the photothermal phase while ϕ_i and σ_i are the normalised measured phase values and their corresponding standard deviations respectively.

As an example, Fig. 6 shows the experimental error bars in addition to experimental data and to the analytical fitting. As for the other samples experimental errors are always less than one degree (typically 0.2–0.4 degrees), the corresponding bars can not be drawn in Fig. 5.

Since a single frequency scanning measurement yields a sequence of averaged data, in principle by using the error propagation theory it would be possible to estimate the uncertainty in the thermal diffusivity evaluation associated to a single test.

However in this work the average value of thermal diffusivity and its uncertainty, as reported in Table IV, have been computed starting from data obtained repeating the experiment more times (usually three) on the same sample.

In particular this uncertainty refers to the mean value standard deviation defined as:

$$\sigma_{\bar{\alpha}} = \sigma_{\alpha_i} / \sqrt{N} \quad (9)$$

4. Results and discussion

Table IV summarises the thermal diffusivity values obtained by fitting the experimental data with Equation 2. For free standing coatings, the reflection coefficient R has been fixed to 1 because the thermal effusivity of air, which acts as substrate, is negligible ($5.51 \text{ W s}^{1/2} \text{ m}^{-2} \text{ K}^{-1}$) if compared to that of the coating. As a matter of fact, effusivity values range between $1900 \text{ W s}^{1/2} \text{ m}^{-2} \text{ K}^{-1}$ (YPSZ) and to $37000 \text{ W s}^{1/2} \text{ m}^{-2} \text{ K}^{-1}$ (Electrolytic copper).

Normalised phase curves measured for all the samples are shown in Figs 5 and 6. The measurements were performed using two different lock-in time constants as a function of the signal amplitude. In particular 300 ms and 1s were used for YPSZ, nickel base alloys and AISI316 and copper, aluminium and iron respectively. The external integration time was of about 40 s. The normalisation of the phase curves was performed on a thermally thick sample of the same material. In such a way the influence of frequency dependence of the detection system and the non-linearity of the IR detector have been minimised.

In Fig. 7 thermal diffusivity values obtained by TWI are compared with data reported in literature: this comparison between expected and measured values gives

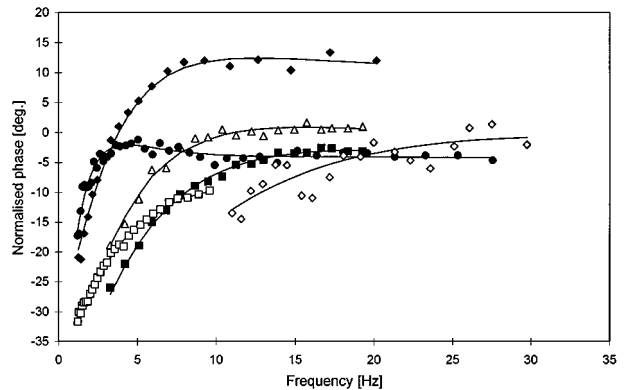


Figure 5 Experimentally measured phase of the ac component of surface temperature versus modulation frequency for APS (●), EBPVD (□), IN738 (■), NIMONIC90 (△), AISI316 (◆) and ARMCO Iron (◇) samples. Solid curves were calculated by Equation 2.

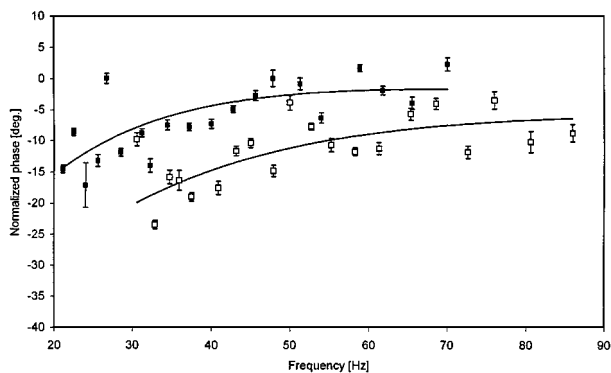


Figure 6 Experimentally measured phase of the ac component of surface temperature versus modulation frequency for UNI3571 (■) and Copper (□) samples. Solid curves were calculated by Equation 2.

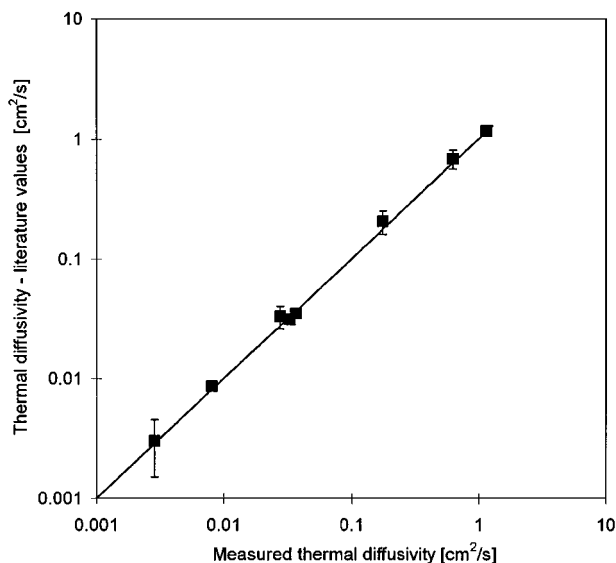


Figure 7 Comparison between thermal diffusivity values measured by TWI method and values as reported in literature. The straight line indicates the perfect agreement between reported and experimentally obtained data. Error bars represent the spreading of thermal diffusivity values found in literature for some materials.

evidence of a very good agreement within a three order of magnitude wide range.

As far as thermal diffusivity of APS sample is concerned, there are many factors participating to the strong spreading of values found in the literature. Main causes are related to porosity content, its shape and its orientation referred to the heat propagation. Moreover the crystalline phase composition of the coating could heavily affect thermal diffusivity values [38].

In particular for this sample, measurements have been carried out both before and after the substrate removal and the difference in thermal diffusivity data resulted to be less than 5%.

5. Conclusions

Experimental results show that TWI can successfully operate requiring a relatively low laser power (lower than 1.5 W) for measuring, in a wide range of values, the thermal diffusivity of thin free standing coatings and single layers. This was allowed because of the approach to the experimental activity we followed. In fact preliminary simulations of experiments using the

three dimensional model have been performed and a subsequent comparison of these results with the one-dimensional model allowed to optimised main experimental parameters.

References

1. A. J. ÅNGSTRÖM, *Phil. Mag.* **25** (1863) 130.
2. M. H. DE SENARMONT, *Annales de Chimie Physique* **3**(2) (1848) 179.
3. W. P. PARKER, R. J. JENKINS, C. P. BUTTER, G. L. GUTTER and G. L. ABBOTT, *J. Appl. Phys.* **32** (1961) 1679.
4. ASTM C714-72 Standard test method for thermal diffusivity of carbon and graphite by a thermal pulse method (1972).
5. BS7134: Section 4.2: 1990; "Method for the determination of thermal diffusivity by the laser flash (or heat pulse) method" (British Standards Institution, 1990).
6. JIS R 1611: Testing methods of thermal diffusivity, specific heat capacity and thermal conductivity for high performance ceramics by laser flash method (Japanese Standards Association, 1991).
7. D. P. ALMOND and P. M. PATEL, "Photothermal Science and Techniques" (Chapman & Hall, London, 1996).
8. G. ROUSSET and F. LEPOUTRE, *Rev. Phys. Appl.* **17** (1982) 201.
9. P. K. KUO, M. J. LIN, C. B. REYES, L. D. FAVRO, R. L. THOMAS, D. S. KIM, S. Y. ZHANG, L. J. INGLEHART, D. FOURNIER, A. C. BOCCARA and N. YACOUBI, *Can. J. Phys.* **64** (1986) 1165.
10. P. K. KUO, E. D. SENDLER, L. F. FAVRO and R. L. THOMAS, *ibid.* **64** (1986) 1168.
11. A. SALAZAR, A. SANCHEZ-LAVEGA and J. FERNANDEZ, *J. Appl. Phys.* **1** (1991) 1216.
12. A. FIGARI, *ibid.* **71** (1992) 3128.
13. *Idem.*, in Proceedings of the Eurotherm Seminar n°27 QIRT 92, Chatenay-Malabry, July 1992, edited by D. Balageas, G. Busse and G. M. Carlomagno (Editions Europeennes Thermique et Industrie, Paris, 1992), p. 377.
14. A. GLAZOV and K. MURATIKOV, *J. Appl. Phys.* **76**(6) (1994) 3279.
15. *Idem.*, *Opt. Eng.* **36**(2) (1997) 358.
16. C. A. BENNETT and R. R. PATTY, *Appl. Opt.* **21** (1982) 49.
17. P. M. PATEL and D. P. ALMOND, *J. Mater. Sci.* **20** (1985) 955.
18. H. P. R. FREDERIKSE, X. T. YING and A. FELDMAN, *Mater. Res. Soc. Symp. Proc.* **142** (1989) 289.
19. L. FABBRI, F. CERNUSCHI, P. FENICI, S. GHIA and G. M. PIANA, in Proceedings of Materials for Advanced Power Engineering, Liege, October 1994, edited by D. Coutsouradis *et al.* (Kluwer, Dordrecht, 1994) Part II, p. 1377.
20. L. FABBRI and P. FENICI, *Rev. Sci. Instrum.* **66**(6) (1995) 3593.
21. L. POTTIER and K. PLAMMAN, *J. Phys. IV C7* (1994) 295.
22. J. OPSAL and A. ROSENCWAIG, *J. Appl. Phys.* **53**(6) (1982) 4240.
23. A. ROSENCWAIG, J. OPSAL, D. L. WILLENBORG, S. M. KELSO and J. T. FANTON, *Appl. Phys. Lett.* **60** (1992) 1301.
24. L. CHEN, J. DING, A. SALNICK, H. CHU, J. OPSAL and A. ROSENCWAIG, in AIP Conference Proceedings n° 463 Photoacoustic and Photothermal Phenomena, Rome, August 1998, edited by F. Scudieri and M. Bertolotti (AIP Woodbury, New York, 1999) p. 102.
25. J. P. ROGER, F. LEPOUTRE, D. FOURNIER and A. C. BOCCARA, *Thin Solid Films* **155** (1987) 165.
26. U. ZAMMIT, F. GASPARINI, M. MARINELLI, R. PIZZOFERRATO, F. SCUDIERI and S. MARTELLUCCI, *J. Appl. Phys.* **69** (1991) 2577.
27. P. CIELO, L. A. UTRACKI and M. LAMONTAGNE, *Can. J. Phys.* **64** (1986) 1172.
28. L. C. AAMODT, J. W. MACLACHLAN SPICER and J. C. MURPHY, *J. Appl. Phys.* **68**(12) (1990) 6087.
29. W. P. LEUNG and A. C. TAM, *ibid.* **56**(1) (1984) 153.
30. L. FABBRI and F. CERNUSCHI, *ibid.* **82**(11) (1997) 5305.

31. UNI 3571 Data sheet.
32. Y. S. TOULOUKIAN, "Thermophysical Properties of High Temperature Solid Materials" Vol. 10 Thermal diffusivity (IFI-PLENUM, New York, 1973).
33. G. BUSSE and H. G. WALTHER, in "Progress in Photothermal and Photoacoustic Science and Technology," edited by A. Mandelis (Elsevier, New York, 1992).
34. INCO. Nimonic 90 Alloy Data Sheet.
35. J. C. MURPHY, J. W. MACLACHLAN and L. C. AAMODT, in "Review of Quantitative Nondestructive Evaluation Vol. 7A," edited by D. O. Thompson and D. E. Chimenti (Plenum Publishing Corporation, New York, 1988).
36. P. BIANCHI, F. CERNUSCHI, A. FIGARI, L. LORENZONI and G. NEGRI, Internal report ENEL SRI-PDM-MAR-98-82.
37. L. PAWLOWSKI, D. LOMBARD, A. MAHLIA, C. MARTIN and P. FAUCHAIS, *High Temp.-High Press* **16** (1984) 347.
38. F. CERNUSCHI, P. BIANCHI, M. LEONI and P. SCARDI, *Journal of Thermal Spray Technology* **8**(1) (1999) 102.

*Received 3 November 1999
and accepted 8 May 2000*